



First-principles investigations of equilibrium calcium isotope fractionation between clinopyroxene and Ca-doped orthopyroxene

Chongqin Feng^{a,b,1}, Tian Qin^{b,c,1}, Shichun Huang^d, Zhongqing Wu^{b,c,*},
Fang Huang^{a,*}

^a CAS Key Laboratory of Crust-Mantle Materials and Environments, School of Earth and Space Sciences, University of Science and Technology of China, Hefei, Anhui 230026, China

^b Laboratory of Seismology and Physics of Earth's Interior, School of Earth and Space Sciences, University of Science and Technology of China, Hefei, Anhui 230026, China

^c Mengcheng National Geophysical Observatory, Anhui, China

^d Department of Geoscience, University of Nevada, 4505 S. Maryland Parkway, Las Vegas, NV 89154, United States

Abstract

Equilibrium fractionation factors of Ca isotopes among mantle minerals are essential for using Ca isotopes as an important tracer in mantle geochemistry. Using the vibrational frequencies obtained by the first-principles calculations based on density functional theory (DFT), we calculated equilibrium fractionation factors of Ca isotopes between two major Ca-bearing minerals, clinopyroxene (cpx) and orthopyroxene (opx). Our results show that opx has much higher $^{44}\text{Ca}/^{40}\text{Ca}$ than its co-existing cpx even at high temperatures (e.g., 1273 K), agreeing with the observations on mantle peridotites. In addition to the well-known temperature effect, our calculations for the first time reveal that the inter-mineral Ca isotope fractionation factor between opx and cpx also has a strong dependence on the chemical composition of opx (i.e., Ca content). Specifically, it increases substantially with decreasing Ca/Mg (atomic ratio) of opx when $\text{Ca/Mg}_{\text{opx}}$ is lower than 1/15. Such compositional effect on inter-mineral Ca isotope fractionation provides a convincing interpretation to the different isotope fractionations between coexisting opx and cpx observed in Kilbourne Hole and San Carlos peridotites.

© 2014 Elsevier Ltd. All rights reserved.

1. INTRODUCTION

Calcium is essential in life and it is also a major rock-forming element in the crust and mantle. Recent analytical advancement has shown great potential for the application

of Ca isotopes in the studies of geological processes at both low and high temperatures (e.g., DePaolo, 2004; Amini et al., 2009; Huang et al., 2009, 2010a,b, 2011, 2012; Simon et al., 2009; Simon and Depaolo, 2010; Schmitt et al., 2012, 2013; Hindshaw et al., 2013; Valdes et al., 2014). Large mass-dependent Ca isotope variation, expressed as $\delta^{44}\text{Ca}$ relative to NIST SRM915a standard ($\delta^{44}\text{Ca} = [((^{44}\text{Ca}/^{40}\text{Ca})_{\text{Sample}} / (^{44}\text{Ca}/^{40}\text{Ca})_{\text{SRM915a}} - 1)] \times 1000(\text{‰})$), has recently been documented in terrestrial igneous rocks. Amini et al. (2009) observed $\sim 0.9\text{‰}$ $^{44}\text{Ca}/^{40}\text{Ca}$ variation in a series of felsic and ultramafic rocks. DePaolo (2004) reported $\sim 0.7\text{‰}$ $^{44}\text{Ca}/^{40}\text{Ca}$ variation in oceanic basalts. More recently, significant Ca isotope variations were observed in mantle minerals and oceanic basalts

* Corresponding authors. Address: Laboratory of Seismology and Physics of Earth's Interior, School of Earth and Space Sciences, University of Science and Technology of China, Hefei, Anhui 230026, China (Z. Wu). Tel.: +86 551 63607810 (F. Huang), +86 551 63607975 (Z. Wu).

E-mail addresses: wuzq10@ustc.edu.cn (Z. Wu), fhuang@ustc.edu.cn (F. Huang).

¹ Co-first author.

(Huang et al., 2010b, 2011; Valdes et al., 2014). These studies clearly indicate that Ca isotopes could be substantially fractionated at high temperature. Therefore, Ca isotopes may provide a novel tool to study a number of fundamental problems such as early planet formation, accretion and evolution of the Earth (Simon and DePaolo, 2010; Huang et al., 2012; Valdes et al., 2014), mantle melting and crustal recycling (DePaolo, 2004; Huang et al., 2011), and thermal and chemical diffusions (Richter et al., 2003; Huang et al., 2010a).

Mantle and crust are the largest reservoirs of Ca in the Earth. Ca Cycles between the mantle and the crust are accomplished by crust growth and recycling (e.g., Plank and Langmuir, 1988, 1993; Hauri et al., 1993; Dasgupta et al., 2004). Recycling of marine carbonates into the mantle through subduction zones can modify the Ca isotope compositions of the mantle because carbonates have distinct $\delta^{44}\text{Ca}$ and much higher Ca content relative to the mantle (DePaolo, 2004; Huang et al., 2011). Since Ca cycles are usually coupled with carbon cycles, Ca isotopes can be used to trace the global carbon cycling over the Earth's history (Zhu and Macdougall, 1998; De La Rocha and DePaolo, 2000; Schmitt et al., 2003; Soudry et al., 2004; Fantle and DePaolo, 2005; Heuser et al., 2005; Kasemann et al., 2005; Steuber and Buhl, 2006; Sime et al., 2007). Consequently, a detailed investigation of the Ca isotope compositions of mantle and crust and how Ca isotopes are fractionated among silicate minerals is necessary.

Huang et al. (2010b) observed variable Ca isotope fractionations between co-existing opx and cpx (defined as $10^3 \ln \alpha_{\text{opx-cpx}} \approx \Delta^{44}\text{Ca}_{\text{opx-cpx}} = \delta^{44}\text{Ca}_{\text{opx}} - \delta^{44}\text{Ca}_{\text{cpx}}$) in mantle peridotites from Kilbourne Hole and San Carlos, 0.75‰ vs. ~0.37‰, respectively. These inter-mineral fractionations are well resolved with the current analytical precision (~0.1‰ for $\delta^{44}\text{Ca}$, 2sd). However, the mechanism for such large and variable inter-mineral Ca isotope differences in mantle peridotites is not well-understood. Possible explanations include equilibrium inter-mineral isotope fractionation at different temperatures and kinetic effects in the upper mantle (Huang et al., 2010b).

To the best of our knowledge, there is no experimental calibration of equilibrium fractionation of Ca isotopes between mantle minerals. Experimental study is challenging because of kinetic fractionations caused by chemical and thermal diffusions during high temperature and pressure experiments (Richter et al., 2003, 2009; Huang et al., 2009, 2010a). Instead, first-principles calculations have been successfully applied to calculate the isotope fractionation factors for a variety of isotope systems including H, O, Li, B, Mg, Si, Cr, Fe, Cu, Mo, and Se (e.g., Anbar et al., 2005; Ottonello and Zuccolini, 2005; Tossell, 2005; Schable et al., 2006; Schable, 2011; Seo et al., 2007; Blanchard et al., 2009; Méheut et al., 2010; Rustad et al., 2010; Kowalski and Jahn, 2011; Kowalski et al., 2013; Li and Liu, 2011; Javoy et al., 2012). We apply this approach to estimate the equilibrium Ca isotope fractionation factor between cpx and opx, the two most important Ca-bearing minerals in the upper mantle. Specifically, we estimated equilibrium Ca isotope fractionations between cpx and opx doped with different amounts of Ca. For the first time,

our results reveal compositional effect on equilibrium fractionation of stable isotopes which are consistent with observations on natural peridotites (Huang et al., 2010b).

2. METHODS

The mass-dependent equilibrium isotope fractionation is controlled by the difference in bond energies, measured with vibrational frequencies, involving the interested element in two phases (Bigeleisen and Mayer, 1947; Urey, 1947). Following Richet et al. (1977), the reduced partition function ratio (β_A) of element X in phase A is the ratio of the isotope compositions of element X in Phase A and that in an ideal mono-atomic gas. Applying the Teller–Redlich rule, β_A in a harmonic approximation is a function of the vibrational frequencies:

$$\beta_A = \left(\frac{Q^*}{Q} \right) = \prod_i^{3N-3} \frac{\mu_i^*}{\mu_i} \frac{e^{-\frac{1}{2}\mu_i^*}}{(1 - e^{-\mu_i^*})} \frac{(1 - e^{-\mu_i})}{e^{-\frac{1}{2}\mu_i}}, \quad (1)$$

where Q represents the vibrational partition function, asterisk refers to the heavy isotope, and i is a running index of vibrational modes. μ_i is defined as:

$$\mu_i = hv_i/k_B T \quad (2)$$

where h is the Plank constant, k_B is the Boltzmann constant, T is the temperature in Kevin, and v_i is the vibrational frequency of the i th mode. There are $3N - 3$ vibrational modes for crystal with N atoms and the product runs over all $3N - 3$ phonon modes. Following Richet et al. (1997), the isotope fractionation factor between phases A and B is usually reported in per mil and is expressed as:

$$\Delta_{A-B} = 10^3 \ln \alpha_{A-B} = 10^3 (\ln \beta_A - \ln \beta_B) \quad (3)$$

Our calculation procedure is similar to that published in previous work (e.g., Li and Liu, 2011; Schable, 2011; Javoy et al., 2012; Huang et al., 2013, 2014). The software package “Quantum Espresso” was employed to calculate the electric structures and vibration frequencies of all minerals (Giannozzi et al., 2009). It uses a plane-wave basis set to expand electronic wave functions and adopts pseudopotential to describe the interaction between the valence electrons and the ionic core. Energy cut-off for plane-waves is 70 Rydberg. The local density approximations (LDA) was used as the exchange-correlation functional (Perdew and Zunger, 1981) because LDA can reproduce experimental observations on the structure and the thermodynamics properties of minerals (e.g., Sholl and Steckel, 2009; Wentzcovitch et al., 2010; Huang et al., 2013). The calculated lattice constants and volume of cpx ($\text{CaMgSi}_2\text{O}_6$) and opx (MgSiO_3) are consistent with literature values within 0.5% (relative difference) (Table 1). Furthermore, as shown in previous work using different approximation functionals (Schable, 2011; Huang et al., 2013), the $10^3 \ln \beta$ of Mg isotopes calculated using the LDA are systematically higher than those calculated using the general gradient approximation functional. However, this offset does not affect the calculated $10^3 \ln \alpha_{A-B}$ because the offsets on $10^3 \ln \beta$ calculated for both phases are cancelled out.

The pseudopotential for Ca was generated following Vanderbilt (1990) with a valence configuration of

Table 1

Crystal lattice parameters. Calculated volume of clinopyroxene and orthopyroxene in this study compared with experimental results.

	<i>a</i> (Å)	<i>b</i> (Å)	<i>c</i> (Å)	α (°)	β (°)	γ (°)	Volume (Å ³)	
Clinopyroxene	9.689	8.828	5.211		105.263		430.005	This study
	9.713	8.857	5.225		105.414		437.37	0 GPa, 300 K ^a
	9.745	8.899	5.251		105.63		438.532	Experiment ^b
	-0.3	-0.5	-0.5		-0.2		-0.3	Difference (%)
Orthopyroxene	18.110	8.755	5.138				814.640	This study
	18.215	8.830	5.174				832.179	0 GPa, 300 K ^a
	18.251	8.814	5.181				833.438	Experiment ^c
	-0.2	0.2	-0.2				-0.2	Difference (%)
Orthopyroxene Ca/Mg = 1/31	18.171	8.755	10.308	90.078	90.053	89.949	1639.953	This study
Orthopyroxene Ca/Mg = 2/30	18.214	8.770	10.290	90.031	90.520	90.047	1643.646	This study
Orthopyroxene Ca/Mg = 2/14	18.283	8.772	5.161	90.000	90.662	90.000	827.659	This study
Orthopyroxene Ca/Mg = 8/8	18.663	8.878	5.244	90.000	90.000	90.000	868.922	This study

^a Data source from Huang et al. (2013).^b Data source from Cameron et al. (1973).^c Data source from Yang and Ghose (1995).

$3s^23p^64s^1$ and a 1.85 Bohr radii cutoff. The pseudopotential for Mg was generated using the method of von Barth and Car (see Dal Corso et al. (1993) for a brief description of the method) with all channels using five valence configurations (followed by weights in the brackets), $3s^23p^0$ (1.5), $3s^13p^1$ (0.6), $3s^13p^{0.5}3d^{0.5}$ (0.3), $3s^13p^{0.5}$ (0.3), and $3s^13d^1$ (0.2), and a cutoff radii of 2.5 Bohr. The O and Si pseudopotentials were generated using the method of Troullier and Martins (1991) with a valence configuration of $2s^22p^4$ and a cutoff radii of 1.45 Bohr for O, and $3s^23p^43d^0$ and 1.47 Bohr for Si.

In our calculations, the primitive cell of opx contains 80 atoms (including 16 Mg atoms), and one or two Mg atoms in the unit cell are replaced by Ca atoms to produce opx with Ca/Mg of 1/15 or 2/14, respectively. In the case of opx with Ca/Mg of 1/31 and 2/30, the primitive unit cell is doubled along the shortest crystal axis so that it contains 160 atoms with 32 Mg atoms, and then one or two Mg atoms are replaced by Ca atoms. The electronic integration was performed by sampling the Brillouin zone with a $1 \times 1 \times 1$ k-point grid for opx (Ca/Mg = 1/31 and 2/30), $1 \times 1 \times 2$ for opx (Ca/Mg = 1/15, 2/14, and 8/8), and $2 \times 2 \times 2$ for cpx to get the converged result (Table S1). Mineral crystals were optimized by exploring variable cell shape molecular dynamics (Wentzcovitch, 1991) and the atomic positions were obtained until the residual forces converge within 5×10^{-4} Ry/Bohr.

The structures with the lowest total energy for various Ca-doped opx are required for calculating the $10^3\ln\beta$ of Ca isotopes. There are two non-equivalent positions for Mg in opx (M_1 and M_2) with M_2 site being larger than M_1 site (12.173 \AA^3 vs. 11.532 \AA^3). The energy difference between Ca in M_2 and M_1 is large (e.g., 0.87 ev for opx with Ca/Mg = 1/15) and Ca in M_2 site is more stable than in M_1 site. Therefore, in our calculations, Ca only occupies M_2 sites in opx. All symmetry-nonequivalent replacements of two M_2 Mg atoms by Ca have been evaluated. The configuration for opx with Ca/Mg of 2/30 in a 160-atom primitive cell with the lowest energy is shown in Fig. 1, which is 0.137 ev lower than that for the 1/15 model in an 80-atom

primitive cell. However, the two configurations (2/30 and 1/15) have similar reduced partition function ratios of Ca isotopes (see Fig. 4), implying that $10^3\ln\beta$ can be accurately obtained using calculations based only on 80-atom cell. For opx with Ca/Mg of 2/14, calculations were done using an 80-atom cell with two Mg atoms in M_2 site being replaced by Ca atoms. Again, all symmetry-nonequivalent replacements of two Mg atoms are explored and the configuration with the lowest energy is shown in Fig. 1.

After the optimized structures for Ca-doped opx were obtained (Fig. 1), their dynamical matrices were calculated on regular q mesh using the density-functional perturbation theory (Baroni et al., 2001). The dynamical matrices were then used to extrapolate a sufficiently dense q mesh to obtain the vibrational density of the state of minerals (Table S1).

3. RESULTS

3.1. Relaxed crystal structure

The structures of opx and cpx are shown in Fig. 1 with emphasis on Mg–O and Ca–O polyhedrons. Mg cations are six-fold coordinated and Ca cations eight-fold in cpx. The coordination number (CN) of Ca in opx depends on the Ca–O bond length threshold taken. If the Ca–O bond length in cpx is used as the threshold, then Ca is six-fold coordinated in opx for all compositions considered in this study (Fig. 2). The structure parameters, such as the cell parameters and volume sizes, obtained with the LDA level are consistent with the results of experimental and other theoretical studies within 0.5% (Table 1), indicating that the volume predicted based on the LDA is reliable. The calculated frequencies for cpx and opx based on LDA agree well with experimental measurement. The frequencies scale factor is 0.9985 with one standard deviation of 0.0253. At high temperature, the error on calculated frequencies would lead to an error of 2 times the deviation on logarithmic β (Méheut et al., 2009). Therefore, the uncertainty on our calculated $10^3\ln\beta$ is estimated at about 5%. Since the $10^3\ln\alpha$ is

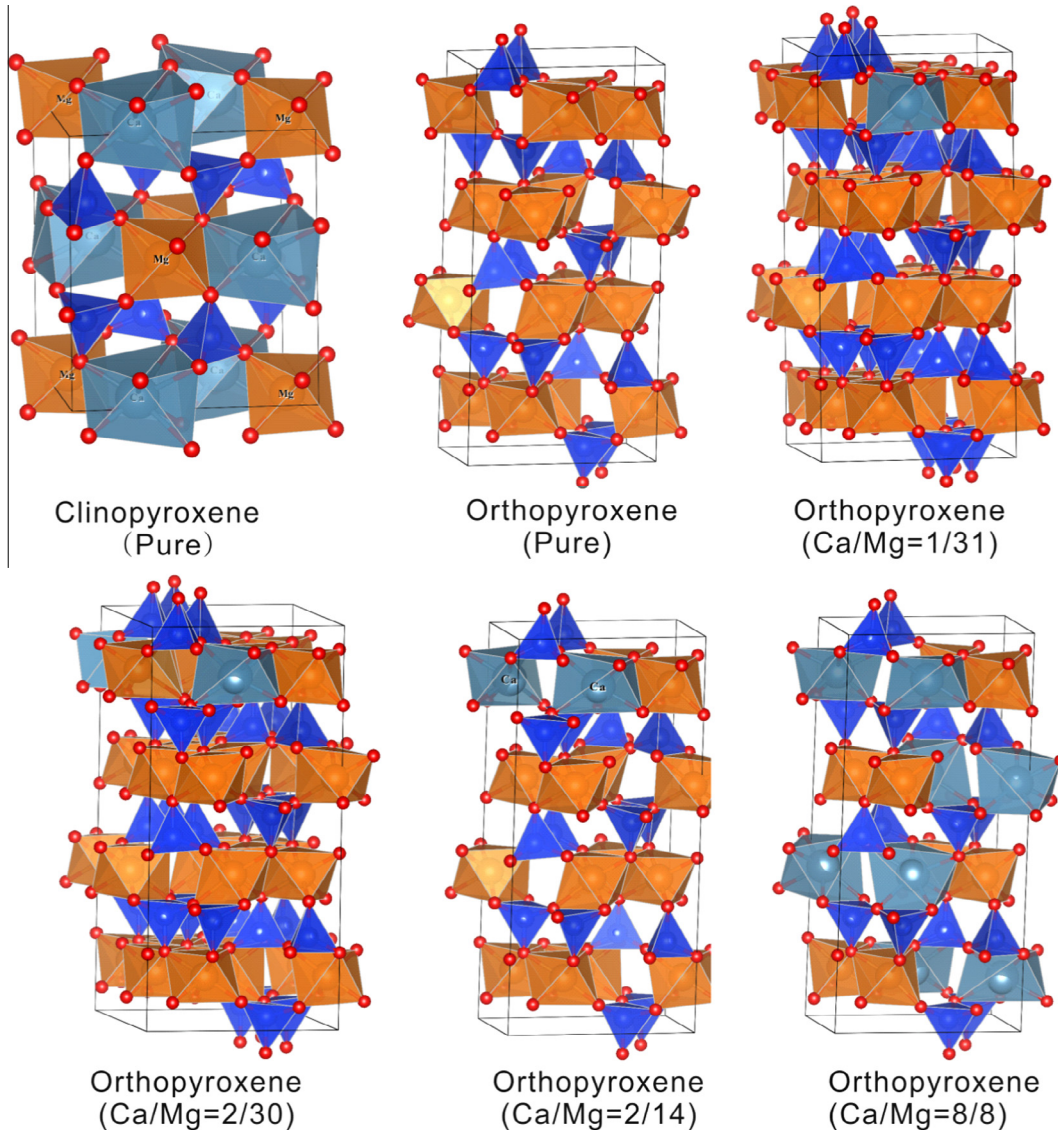


Fig. 1. The crystal structures of diopside (cpx) ($VIII^{VI}Ca^{VI}MgSi_2O_6$, Ca:Mg = 1:1), orthopyroxene ($V^{VI}MgSiO_3$), and orthopyroxenes ($V^{VI}Ca^{VI}MgSi_2O_6$) with Ca/Mg (atomic) ratios of 1/31, 2/30, 2/14, and 8/8. Ca cations are cyan, Mg, brown; O, red; and Si, blue. The Mg–O polyhedrons in diopside are deformed. The structures of Ca-free orthopyroxene and diopside are in good agreement with the results of previous work (e.g., Huang et al., 2013), indicating that the crystal models of this study are reliable. All of these crystal structures are drawn by the software “VESTA” (Momma and Izumi, 2008). (For interpretation of the references to colour in this figure legend, the reader is referred to the web version of this article.)

the difference of two $10^3\ln\beta$, the uncertainty of $10^3\ln\alpha$ is about 7% (Méheut et al., 2009; Kowalski et al 2013).

The structure of the Ca-doped opx is substantially different from the undoped opx. As shown in Fig. 2, lengths of the individual Ca–O and Mg–O bonds range from 2.221 to 2.533 Å and 1.986 to 2.440 Å, respectively. The average Ca–O bond length increases with increasing Ca proportion in opx when Ca/Mg is lower than 2/14, while it becomes insensitive to Ca proportion when Ca/Mg is greater than 2/14 (Fig. 2). The average Mg–O bond lengths in opx do not vary with Ca/Mg, implying that $10^3\ln\beta$ of Mg isotopes in opx are not sensitive to major element compositions. In summary, Ca–O bond length in opx is always shorter than

those in cpx, and it varies with Ca/Mg in opx. In contrast, Mg–O bond length in opx is nearly identical to that in cpx.

3.2. Ca isotope fractionation factors

Polynomial fitting factors of the reduced partition function ratios of $^{44/40}\text{Ca}$ ($10^3\ln\beta^{44-40}$) and the inter-mineral fractionation factors ($10^3\ln\alpha_{\text{oxp}-\text{cpx}}$) are reported in Tables 3 and 4, respectively. They are plotted as a function of temperature in Fig. 3. At the same temperature, $10^3\ln\beta^{44-40}$ of opx is always larger than $10^3\ln\beta^{44-40}$ of cpx. Notably, $10^3\ln\beta^{44-40}$ of opx increases with decreasing Ca/Mg especially when Ca/Mg is lower than 1/15. Therefore, $10^3\ln\alpha_{\text{oxp}-\text{cpx}}$ is

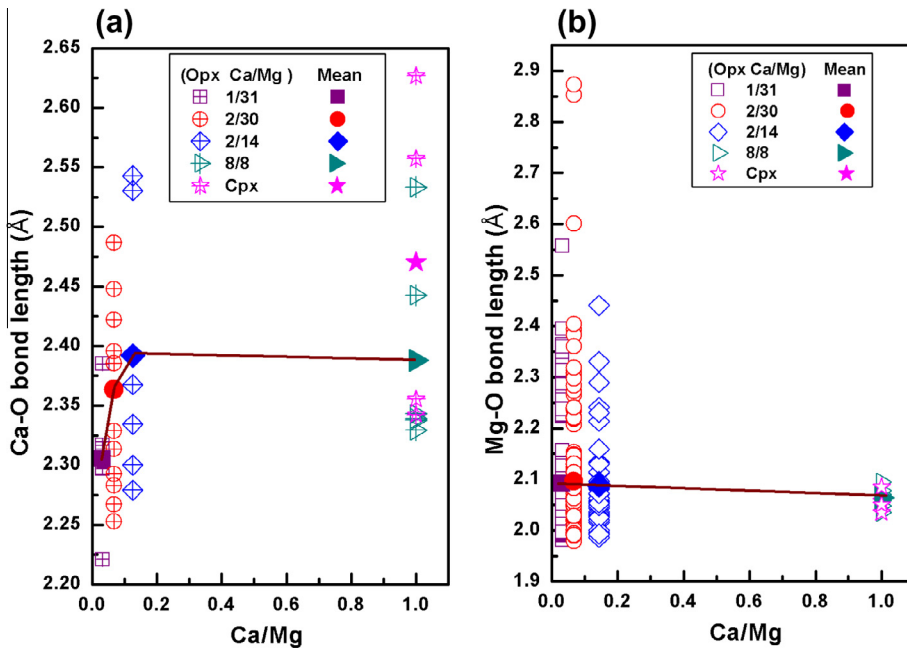


Fig. 2. (a) Ca–O bond lengths of diopside ($\text{CaMgSi}_2\text{O}_6$) and opx ($\text{Ca}_x\text{Mg}_{2-x}\text{Si}_2\text{O}_6$) versus Ca/Mg (atomic ratio). The solid lines show that average bond lengths of Ca–O in opx vary with Ca/Mg. (b) Mg–O bond lengths in diopside and opx versus Ca/Mg (atomic ratio). The average Mg–O bond lengths of opx and cpx do not vary with Ca/Mg.

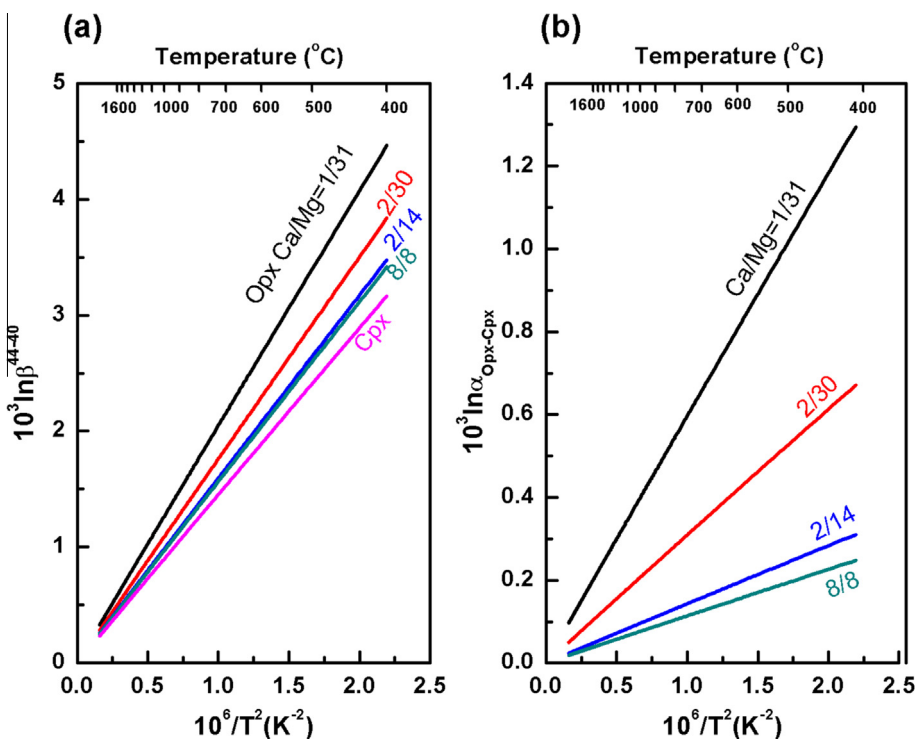


Fig. 3. (a) Ca isotope β -factors of Ca-doped opx and diopside obtained from Eq. (1). (b) Temperature dependence of the $10^3 \ln \alpha_{\text{oxp}-\text{cpx}}$ of Ca isotopes. Opx is always enriched in heavier Ca isotopes relative to cpx.

not only controlled by temperature, but also varies significantly with Ca/Mg in opx. As further illustrated in Fig. 4, $10^3 \ln \alpha_{\text{oxp}-\text{cpx}}$ decreases almost linearly with increasing average Ca–O bond length in opx, which is related to $\text{Ca/Mg}_{\text{oxp}}$

when Ca is a minor element. The Ca CN in opx depends on the Ca–O bond length threshold taken. In opx, the average Ca–O bond length of the six shortest Ca–O bonds is linearly correlated with Ca isotope fractionation factors (Fig. 4).

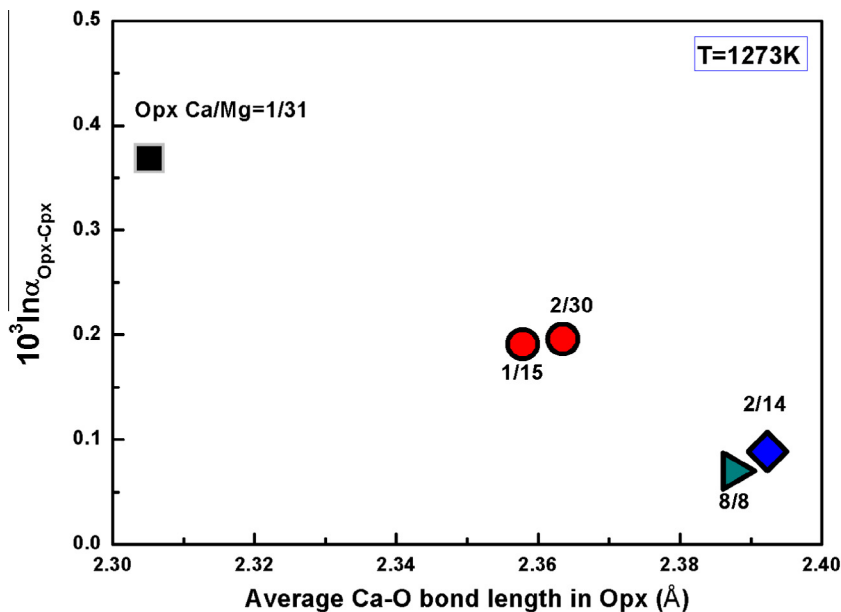


Fig. 4. Negative correlation between $10^3 \ln\alpha_{Opx-Cpx}$ (%) of Ca isotopes and average Ca–O bond length in opx at 1273 K. Ca substitution for Mg can affect the average Ca–O bond length of opx when Ca/Mg is low, while the average bond length does not significantly vary when $\text{Ca/Mg}_{\text{opx}} > 2/14$. Note that the Ca–O bond length for opx with Ca/Mg of 1/15 (based on an 80-atom unit cell) agrees well with that of opx with Ca/Mg of 2/30 calculated from a 160-atom cell.

Table 2
Average Ca–O and Mg–O bond lengths in cpx and opx.

Mineral	Average bond length (Å)					
	Ca/Mg	Ca–O			Mg–O	
		This study ^a	Smyth and Bish (1988)	Shannon (1976)	This study	Shannon (1976)
Clinopyroxene $\text{VIII}\text{Ca}^{\text{VI}}\text{MgSi}_2\text{O}_6$	8/8	2.470	2.50	2.48 ^b 2.50 ^b	2.057	
Orthopyroxene $\text{Ca}_x\text{Mg}_{(1-x)}\text{Si}_2\text{O}_6$	1/31	2.305	2.15	2.36(8) ^c	2.092	2.08 ^d
	1/15	2.358			2.096	2.10 ^d
	2/30	2.363			2.096	
	2/14	2.392			2.088	
	8/8	2.388			2.064	

Clinopyroxene is calculated based on the formula of $\text{CaMgSi}_2\text{O}_6$.

^a Ca is eight-fold coordinated in cpx, we calculate the average of six bond lengths in opx.

^b O^{2-} has both four-fold and three-fold coordination sites in pyroxenes (Ashbrook et al., 2002). $\text{Ca}^{\text{VIII}}-\text{O}^{\text{III}}(\text{r}(\text{Ca}^{\text{VIII},2+}) + \text{r}(\text{O}^{\text{III},2-}))$ is 2.48 Å and $\text{Ca}^{\text{VIII}}-\text{O}^{\text{IV}}(\text{r}(\text{Ca}^{\text{VIII},2+}) + \text{r}(\text{O}^{\text{IV},2-}))$ is 2.50 Å.

^c $\text{Ca}^{\text{VI}}-\text{O}^{\text{III}}$ is 2.36 Å and $\text{Ca}^{\text{VI}}-\text{O}^{\text{IV}}$ is 2.38 Å.

^d $\text{Mg}^{\text{VI}}-\text{O}^{\text{III}}$ is 2.08 Å and $\text{Mg}^{\text{VI}}-\text{O}^{\text{IV}}$ is 2.10 Å.

Table 3

Calculated reduced partition function ratios of $^{44}\text{Ca}/^{40}\text{Ca}$ (1000 $\ln\beta$) for clinopyroxene and orthopyroxene with different Ca/Mg atomic ratios.

Minerals	Ca/Mg	a	b	c
Orthopyroxene	1/31	2.06065	-0.01265	1.88286E-4
	2/30	1.77799	-0.00971	1.50828E-4
	2/14	1.60256	-0.00827	1.30891E-4
	8/8	1.57271	-0.0077	1.20247E-4
Clinopyroxene	8/8	1.45802	-0.00689	1.17851E-4

$1000\ln\beta = ax + bx^2 + cx^3$, where $x = 10^6/T^2$. T is temperature in Kelvin. The parameters a, b, and c are fitted between 673 K and 2498 K.

Table 4

Fitting of $10^3 \ln \alpha_{\text{Opx-Cpx}}$ for orthopyroxenes with different Ca/Mg with temperature ranging from 673 K to 2498 K.

Element	Ca/Mg (atomic ratio)	$10^3 \ln \alpha = a \times (10^6/T^2) + b \times (10^6/T^2)^2 + c \times (10^6/T^2)^3$		
		a	b	c
$^{44}\text{Ca}/^{40}\text{Ca}$	1/31	0.60263	-0.00575	7.04358E-5
	2/30	0.31997	-0.00282	3.29774E-5
	2/14	0.14454	-0.00138	1.30405E-5
	8/8	0.11469	-8.0481E-4	2.39649E-6

T is temperature in Kelvin.

The seventh and eighth Ca–O bonds are too long (and too weak) to generate observable effect on isotope fractionation factors, so that they are not included in calculating the average Ca–O bond length in opx.

4. DISCUSSION

4.1. Influence of Ca substitution on equilibrium Ca isotope fractionation

Our results show that $10^3 \ln \alpha_{\text{Opx-cpx}}$ is controlled by the proportion of Ca substitution in opx (Fig. 4). The effect of variable Ca/Mg in diopside (cpx) is not considered because of its limited variation in natural cpx. $10^3 \ln \alpha_{\text{Opx-cpx}}$ is very sensitive to Ca/Mg in opx when $\text{Ca/Mg} < 1/15$, and becomes less sensitive to Ca/Mg in opx when $\text{Ca/Mg} > 2/14$. The average Ca–O bond length and $10^3 \ln \alpha_{\text{Opx-cpx}}$ for opx with a Ca/Mg of 2/14 are almost identical to that of opx with a Ca/Mg of 8/8.

Isotope fractionation is controlled by bonding strength (e.g., Bigeleisen and Mayer, 1947; Urey, 1947; Chacko et al., 2001). A shorter chemical bond has stronger bonding strength and higher vibrational frequency, and thus it is enriched in heavy isotopes relative to a longer and weaker bond. The relationship between bond-length and isotope fractionation has been discussed for many stable isotopes such as Li, Mg, Cr, Fe, and Ge isotopes (e.g., Schauble et al., 2004; Hill and Schauble, 2008; Li et al., 2009; Young et al., 2009; Wunder et al., 2011). For Ca isotopes, this correlation has been shown between Ca-bearing minerals and seawater (Griffith et al., 2008), cpx and opx pairs, and among calcite, aragonite and barite (Gussone et al., 2005; Huang et al., 2010b).

The bond lengths of $\text{Ca}^{\text{VI}}-\text{O}^{\text{II}}$ and $\text{Ca}^{\text{VI}}-\text{O}^{\text{III}}$ in opx were taken as 2.36 Å and 2.38 Å, respectively, by Shannon (1976) without considering the chemical effect on bond length. This approach is over-simplified because the average Ca–O bond length in opx varies with its Ca proportion (Figs. 2, 4, and Table 2). When Ca is a major element in a crystal, Ca–Mg substitution does not generate observable changes in the average Ca–O bond length. The relatively small change in Ca/Mg in cpx does not modify its polyhedron shape and structure parameters. This is probably because Ca cation is much bigger than Mg cation and thus the Ca–O bond length cannot be significantly modified as Ca is a major element in the mineral. However, when Ca is a minor element in opx, the average Ca–O bond length is sensitive to the adjacent environment of Ca cation in

the mineral structure. A lower Ca/Mg in opx leads to a shorter Ca–O bond length and thus enrichment of heavy Ca isotopes in opx (Fig. 4). Since the average Ca–O bond length controls $10^3 \ln \alpha_{\text{Opx-cpx}}$ (Fig. 4), Ca–Mg substitution in opx plays an important role in controlling Ca isotope fractionation between opx and cpx. This explains the observation that a small change in Ca/Mg from 0.017 in Kilbourne Hole opx to 0.022 in San Carlos opx accompanies a dramatic decrease in $10^3 \ln \alpha_{\text{Opx-cpx}}$ from 0.75‰ to 0.37‰ (Huang et al., 2010b).

4.2. Ca isotope fractionation between cpx and opx

Understanding Ca isotope fractionation in igneous rock is essential for applying Ca isotopes in the study of mantle geochemistry, such as the role of subducted materials in metasomatizing the mantle sources of oceanic basalts. Huang et al. (2010b) reported that the average $\delta^{44}\text{Ca}$ of opx in Kilbourne Hole and San Carlos mantle peridotites are $1.73 \pm 0.09\text{‰}$ and $1.40 \pm 0.07\text{‰}$, respectively, while the average $\delta^{44}\text{Ca}$ of cpx are $0.98 \pm 0.04\text{‰}$ and $1.04 \pm 0.04\text{‰}$, respectively. Although equilibrium temperatures of these two peridotite xenoliths are $\sim 1000\text{ }^\circ\text{C}$ as estimated by two pyroxene elemental thermometry, it is not clear why $10^3 \ln \alpha_{\text{Opx-cpx}}$ shows a large variation from 0.36‰ to 0.75‰. Two possible explanations were provided in Huang et al. (2010b).

- (1) The different $10^3 \ln \alpha_{\text{Opx-cpx}}$ may reflect isotope disequilibrium between opx and cpx due to kinetic effect such as chemical diffusion. However, this is inconsistent with the observation that no compositional zoning was found in the pyroxenes from San Carlos and Kilbourne Hole peridotites (Huang et al., 2010b). Since isotope equilibrium is achieved faster than chemical equilibrium (e.g., Lesher 1990; van der Laan et al., 1994), the lack of chemical disequilibrium (e.g., Galer and Onions, 1989) rules out the possibility that the cpx–opx pairs at San Carlos and Kilbourne Hole did not reach isotope equilibrium. Such conclusion is also supported by oxygen isotope studies on San Carlos peridotites (e.g., Eiler et al., 1995; Eiler, 2001). Consequently, the different $10^3 \ln \alpha_{\text{Opx-cpx}}$ reported in Huang et al. (2010b) do not likely reflect kinetic effect.
- (2) The variable $10^3 \ln \alpha_{\text{Opx-cpx}}$ may reflect equilibrium isotope fractionation at different temperatures. To the first order, equilibrium fractionation is a linear

function of $1/T^2$ with T being temperature in Kelvin (Bigeleisen and Mayer, 1947; Criss, 1991). The difference in $10^3 \ln \alpha_{\text{opx-cpx}}$ (0.36% vs. 0.75%) can thus be translated into a temperature difference of a factor of 1.4. However, the pyroxene equilibration temperature is 1295 ± 34 K for San Carlos peridotites (Galer and Onions, 1989) and 1276 ± 58 K for Kilbourne Hole peridotites (e.g., Galer and Onions, 1989; Bussod and Williams, 1991; Hamblock et al., 2007). Therefore, the large variation in $10^3 \ln \alpha_{\text{opx-cpx}}$ cannot be caused by temperature difference.

Our results provide an explanation for the variation of $10^3 \ln \alpha_{\text{opx-cpx}}$ in San Carlos and Kilbourne Hole peridotites. As discussed above in Sections 3.2 and 4.1, our calculation demonstrates that the proportion of Ca substitution (Ca/Mg) in opx influences the equilibrium Ca isotope fractionation between two pyroxenes, especially when Ca/Mg in opx is $<1/15$. Ca/Mg is usually low in natural opx in peridotites. Ca/Mg_{opx} in San Carlos and Kilbourne Hole peridotites are 0.022 and 0.017, respectively (Huang et al., 2010b). According to our results, $10^3 \ln \alpha_{\text{opx-cpx}}$ increases rapidly from 0.19% to 0.37% when Ca/Mg_{opx} decreases from 0.0667 to 0.0323 (i.e., Ca/Mg = 2/30 and 1/31) at 1273 K (see Fig. 5). The measured $10^3 \ln \alpha_{\text{opx-cpx}}$ in Kilbourne Hole peridotite plots slightly above the 1273 K fit curve in Fig. 5, which

could reflect the large uncertainty caused by extrapolating our first-principle calculation results. Nevertheless, based on our calculation, we propose that the variable $10^3 \ln \alpha_{\text{opx-cpx}}$ for the San Carlos and Kilbourne Hole peridotites reflect equilibrium isotope fractionations at similar temperature but with different proportions of Ca substitution in opx.

4.3. A potential opx–cpx Ca isotope thermometry

The relationship between Ca/Mg in opx and Ca isotope fractionation is shown in Fig. 5. At a given temperature, Ca isotope fractionation between cpx and opx is significant compared to the current analytical precision, especially when Ca/Mg_{opx} is low. Since $10^3 \ln \alpha_{\text{opx-cpx}}$ is sensitive to temperature, it is possible to use Ca isotope fractionation between opx and cpx as a two pyroxene Ca isotope geothermometry. For example, if Ca/Mg of opx is 1/31, $10^3 \ln \alpha_{\text{opx-cpx}}$ decreases from 0.78% to 0.36% with temperature increasing from 873 K to 1273 K. Such geothermometry is more accurate if cpx is in equilibrium with the opx with a lower Ca/Mg. This may provide a useful tool to estimate temperature for rocks with coexisting opx and cpx such as peridotite and pyroxenite. Future studies of experimental calibration or theoretical calculation on opx with lower Ca/Mg are needed to fully establish such new thermometry.

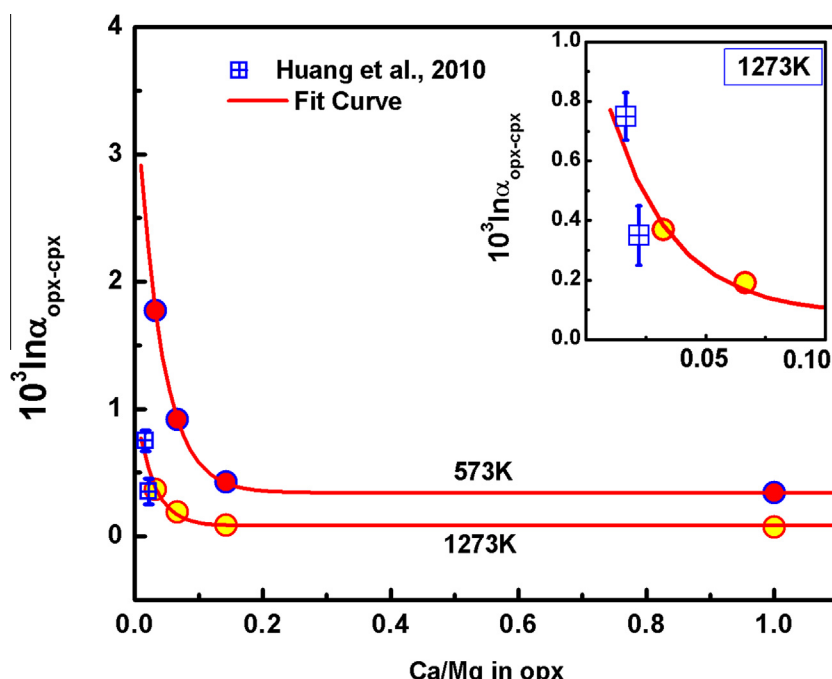


Fig. 5. Correlation between $10^3 \ln \alpha_{\text{opx-cpx}}$ and Ca/Mg_{opx}. $10^3 \ln \alpha_{\text{opx-cpx}}$ increases dramatically with decreasing Ca/Mg_{opx} when Ca/Mg is $\leq 1/15$. Blue open squares represent observations in the Kilbourne Hole and San Carlos mantle peridotites (Huang et al., 2010b), indicating that samples with similar equilibrium temperatures can have distinct Ca isotope fractionations. The equation of the red fitting line is shown in Table S2. Error of Ca/Mg is 0.0066 and 0.0015 for the Kilbourne Hole and San Carlos mantle peridotites, respectively, similar to the size of the symbols. (For interpretation of the references to colour in this figure legend, the reader is referred to the web version of this article.)

5. CONCLUSIONS

First-principles calculation of Ca isotope fractionation factors between opx and cpx shows that opx is more enriched in heavy Ca isotopes than cpx, agreeing with observations on peridotite xenoliths. Our calculation reveals that $10^3 \ln \alpha_{\text{oxp}-\text{cpx}}$ increases with decreasing Ca/Mg in opx especially when Ca is a minor element. This indicates that different proportion of Ca substitution in opx can influence the crystal parameters such as average Ca–O bond length and strength, which further affects $10^3 \ln \alpha_{\text{oxp}-\text{cpx}}$. Our results provide a compelling explanation for the variable $10^3 \ln \alpha_{\text{oxp}-\text{cpx}}$ observed in Kilbourne Hole and San Carlos mantle peridotites. Because Ca/Mg (atomic ratio) of opx from these two peridotites are low, a slight decrease of Ca/Mg (from 0.022 to 0.017) in opx could dramatically increase $10^3 \ln \alpha_{\text{oxp}-\text{cpx}}$. Finally, since $10^3 \ln \alpha_{\text{oxp}-\text{cpx}}$ is large relative to the current analytical error and sensitive to both temperature and chemical composition of opx, if carefully calibrated, Ca isotope fractionation between opx and cpx can be used as a potential two-pyroxene Ca isotope thermometry.

ACKNOWLEDGMENTS

We thank two anonymous referees for their constructive comments which significantly improve the manuscript, and Marc Norman, Weidong Sun, and Fang-Zhen Teng for their editorial handling. This work is supported by State Key Development Program of Basic Research of China (2014CB845905), the Natural Science Foundation of China (41173031, 41274087, and 41090370), the Chinese Academy of Sciences International Partnership Program for Creative Research Teams and the 111 project. S.H. is supported by NSF Grant EAR-1144727. The computations were operated in Shanghai supercomputer center.

APPENDIX A. SUPPLEMENTARY DATA

Supplementary data associated with this article can be found, in the online version, at <http://dx.doi.org/10.1016/j.gca.2014.06.002>.

REFERENCES

- Amini M., Eisenhauer A., Bohm F., Holmden C., Kreissig K., Hauff F. and Jochum K. P. (2009) Calcium isotopes (delta Ca-44/40) in MPI-DING reference glasses, USGS rock powders and various rocks: evidence for Ca isotope fractionation in terrestrial silicates. *Geostand. Geoanal. Res.* **33**, 231–247.
- Anbar A. D., Jarzecki A. A. and Spiro T. G. (2005) Theoretical investigation of iron isotope fractionation between Fe(H₂O)(3+)(6) and Fe(H₂O)(2+)(6): implications for iron stable isotope geochemistry. *Geochim. Cosmochim. Acta* **69**, 825–837.
- Ashbrook S. E., Berry A. J. and Wimperis S. (2002) O-17 multiple-quantum MAS NMR study of pyroxenes. *J. Phys. Chem. B* **106**, 773–778.
- Baroni S., de Gironcoli S., Dal Corso A. and Giannozzi P. (2001) Phonons and related crystal properties from density-functional perturbation theory. *Rev. Mod. Phys.* **73**, 515–562.
- Bigeleisen J. and Mayer M. G. (1947) Calculation of equilibrium constants for isotopic exchange reactions. *J. Chem. Phys.* **15**, 261–267.
- Blanchard M., Poitrasson F., Meheut M., Lazzeri M., Mauri F. and Balan E. (2009) Iron isotope fractionation between pyrite (FeS₂), hematite (Fe₂O₃) and siderite (FeCO₃): a first-principles density functional theory study. *Geochim. Cosmochim. Acta* **73**, 6565–6578.
- Bussod G. Y. A. and Williams D. R. (1991) Thermal and kinematic model of the southern Rio Grande rift: inferences from crustal and mantle xenoliths from Kilbourne Hole, New Mexico. *Tectonophysics* **197**, 373–389.
- Cameron M., Sueno S., Prewitt C. T. and Papike J. J. (1973) High-temperature crystal-chemistry of acmite, diopside, hedenbergite, jadeite, spodumene, and ureyite. *Am. Mineral.* **58**(7–8), 594–618.
- Chacko T., Cole D. R. and Horita J. (2001) Equilibrium oxygen, hydrogen and carbon isotope fractionation factors applicable to geologic systems. *Rev. Mineral. Geochem.* **43**, 1–82.
- Criss R.E. (1991) Temperature dependence of isotopic fractionation factors. In *Stable Isotope Geochemistry: A Tribute to Samuel Epstein* Vol. 3, pp11–16.
- Dal Corso A., Baroni S., Resta R. and de Gironcoli S. (1993) Ab initio calculation of phonon dispersions in II–VI semiconductors. *Phys. Rev. B* **47**, 3588.
- Dasgupta R., Hirschmann M. M. and Withers A. C. (2004) Deep global cycling of carbon constrained by the solidus of anhydrous, carbonated eclogite under upper mantle conditions. *Earth Planet. Sci. Lett.* **227**, 73–85.
- De La Rocha C. L. and DePaolo D. J. (2000) Isotopic evidence for variations in the marine calcium cycle over the Cenozoic. *Science* **289**, 1176–1178.
- DePaolo D. J. (2004) Calcium isotopic variations produced by biological, kinetic, radiogenic and nucleosynthetic processes. In *Geochemistry of Non-Traditional Stable Isotopes* (eds. C. M. Johnson, B. L. Beard and F. Albarede). Mineralogical Soc. America, Washington, pp. 255–288.
- Eiler J. M. (2001) Oxygen isotope variations of basaltic lavas and upper mantle rocks. In: *Stable Isotope Geochemistry* (eds. J. W. Valley and D. R. Cole). pp. 319–364.
- Eiler J. M., Farley K. A., Valley J. W., Stolper E. M., Hauri E. H. and Craig H. (1995) Oxygen-isotope evidence against bulk recycled sediment in the mantle sources of Pitcairn Island lavas. *Nature* **377**, 138–141.
- Galer S. J. G. and Onions R. K. (1989) Chemical and isotopic studies of ultramafic inclusions from the San-Carlos volcanic field, Arizona – a bearing on their petrogenesis. *J. Petrol.* **30**, 1033–1064.
- Fantle M. S. and DePaolo D. J. (2005) Variations in the marine Ca cycle over the past 20 million years. *Earth Planet. Sci. Lett.* **237**, 102–117.
- Giannozzi P., Baroni S., Bonini N., Calandra M., Car R., Cavazzoni C., Ceresoli D., Chiarotti G. L., Cococcioni M., Dabo I., Dal Corso A., de Gironcoli S., Fabris S., Fratesi G., Gebauer R., Gerstmann U., Gougauss C., Kokalj A., Lazzeri M., Martin-Samos L., Marzari N., Mauri F., Mazzarello R., Paolini S., Pasquarello A., Paulatto L., Sbraccia C., Scandolo S., Scelazero G., Seitsonen A. P., Smogunov A., Umari P. and Wentzcovitch R. M. (2009) QUANTUM ESPRESSO: a modular and open-source software project for quantum simulations of materials. *J. Phys. Condens. Matter* **21**.
- Griffith E. M., Schauble E. A., Bullen T. D. and Paytan A. (2008) Characterization of calcium isotopes in natural and synthetic barite. *Geochim. Cosmochim. Acta* **72**, 5641–5658.
- Gussone N., Bohm F., Eisenhauer A., Dietzel M., Heuser A., Teichert B. M. A., Reitner J., Worheide G. and Dullo W. C. (2005) Calcium isotope fractionation in calcite and aragonite. *Geochim. Cosmochim. Acta* **69**, 4485–4494.

- Hamblock J. M., Andronicos C. L., Miller K. C., Barnes C. G., Ren M. H., Averill M. G. and Anthony E. Y. (2007) A composite geologic and seismic profile beneath the southern Rio Grande rift, New Mexico, based on xenolith mineralogy, temperature, and pressure. *Tectonophysics* **442**, 14–48.
- Hauri E. H., Shimizu N., Dieu J. J. and Hart S. R. (1993) Evidence for hotspot-related carbonatite metasomatism in the oceanic upper-mantle. *Nature* **365**, 221–227.
- Heuser A., Eisenhauer A., Boehm F., Wallmann K., Gussone N., Pearson P. N., Naegler T. F. and Dullo W.-C. h. (2005) Calcium isotope ($d_{44}/40\text{Ca}$) variations of Neogene planktonic foraminifera. *Paleoceanography* **20**, PA2013. <http://dx.doi.org/10.1029/2004PA001048>.
- Hindshaw R. S., Reynolds B. C., Wiederhold J. G., Kiczka M., Kretzschmar R. and Bourdon B. (2013) Calcium isotope fractionation in alpine plants. *Biogeochemistry* **112**, 373–388.
- Hill P. S. and Schauble E. A. (2008) Modeling the effects of bond environment on equilibrium iron isotope fractionation in ferric aquo-chloro complexes. *Geochim. Cosmochim. Acta* **72**, 1939–1958.
- Huang F., Lundstrom C. C., Glessner J., Ianno A., Boudreau A., Li J., Ferre E. C., Marshak S. and DeFrates J. (2009) Chemical and isotopic fractionation of wet andesite in a temperature gradient: experiments and models suggesting a new mechanism of magma differentiation. *Geochim. Cosmochim. Acta* **73**, 729–749.
- Huang F., Chakraborty P., Lundstrom C. C., Holmden C., Glessner J. J. G., Kieffer S. W. and Lesher C. E. (2010a) Isotope fractionation in silicate melts by thermal diffusion. *Nature* **464**, 396–400.
- Huang S., Farkas J. and Jacobsen S. B. (2010b) Calcium isotopic fractionation between clinopyroxene and orthopyroxene from mantle peridotites. *Earth Planet. Sci. Lett.* **292**, 337–344.
- Huang S., Farkas J. and Jacobsen S. B. (2011) Stable calcium isotopic compositions of Hawaiian shield lavas: evidence for recycling of ancient marine carbonates into the mantle. *Geochim. Cosmochim. Acta* **75**, 4987–4997.
- Huang S., Farkas J., Yu G., Petaei M. I. and Jacobsen S. B. (2012) Calcium isotopic ratios and rare earth element abundances in refractory inclusions from the Allende CV3 chondrite. *Geochim. Cosmochim. Acta* **77**, 252–265.
- Huang F., Chen L., Wu Z. and Wang W. (2013) First-principles calculations of equilibrium Mg isotope fractionations between garnet, clinopyroxene, orthopyroxene, and olivine: implications for Mg isotope thermometry. *Earth Planet. Sci. Lett.* **367**, 61–70.
- Huang F., Wu Z., Huang S. and Wu F. (2014). First-principles calculations of equilibrium silicon isotope fractionation among mantle minerals. *Geochim. Cosmochim. Acta* (in press).
- Javoy M., Balan E., Meheut M., Blanchard M. and Lazzeri M. (2012) First-principles investigation of equilibrium isotopic fractionation of O- and Si-isotopes between refractory solids and gases in the solar nebula. *Earth Planet. Sci. Lett.* **319**, 118–127.
- Kasemann S. A., Hawkesworth Ch. J., Pravec A. R., Fallick P. N. and Pearson P. N. (2005) Boron and calcium isotope composition in Neoproterozoic carbonate rocks from Namibia: evidence for extreme environmental change. *Earth Planet. Sci. Lett.* **231**, 73–86.
- Kowalski P. M. and Jahn S. (2011) Prediction of equilibrium Li isotope fractionation between minerals and aqueous solutions at high P and T: an efficient ab initio approach. *Geochim. Cosmochim. Acta* **75**, 6112–6123.
- Kowalski P. M., Wunder B. and Jahn S. (2013) Ab initio prediction of equilibrium boron isotope fractionation between minerals and aqueous fluids at high P and T. *Geochim. Cosmochim. Acta* **101**, 285–301.
- Lesher C. E. (1990) Decoupling of chemical and isotopic exchange during magma mixing. *Nature* **344**, 235–237.
- Li X. and Liu Y. (2011) Equilibrium Se isotope fractionation parameters: a first-principles study. *Earth Planet. Sci. Lett.* **304**, 113–120.
- Li X., Zhao H., Tang M. and Liu Y. (2009) Theoretical prediction for several important equilibrium Ge isotope fractionation factors and geological implications. *Earth Planet. Sci. Lett.* **287**, 1–11.
- Méheut M., Lazzeri M., Balan E. and Mauri F. (2009) Structural control over equilibrium silicon and oxygen isotopic fractionation: a first-principles density-functional theory study. *Chem. Geol.* **258**, 28–37.
- Meheut M., Lazzeri M., Balan E. and Mauri F. (2010) First-principles calculation of H/D isotopic fractionation between hydrous minerals and water. *Geochim. Cosmochim. Acta* **74**, 3874–3882.
- Momma K. and Izumi F. (2008) VESTA: a three-dimensional visualization system for electronic and structural analysis. *J. Appl. Crystallogr.* **41**, 653–658.
- Ottanello G. and Zuccolini M. V. (2005) Ab-initio structure, energy, and stable Cr isotopes equilibrium fractionation of some geochemically relevant H–O–Cr–Cl complexes. *Geochim. Cosmochim. Acta* **69**, 851–874.
- Perdew J. P. and Zunger A. (1981) Self-interaction correction to density-functional approximations for many-electron systems. *Phys. Rev. B* **23**, 5048–5079.
- Plank T. and Langmuir C. H. (1988) An evaluation of the global variations in the major element chemistry of arc basalts. *Earth Planet. Sci. Lett.* **90**, 349–370.
- Plank T. and Langmuir C. H. (1993) Tracing trace elements from sediment input to volcanic output at subduction zones. *Nature* **362**, 739–743.
- Richert P., Bottinga Y. and Javoy M. (1977) Review of hydrogen, carbon, nitrogen, oxygen, sulfur, and chlorine stable isotope fractionation among gaseous molecules. *Annu. Rev. Earth Planet. Sci.* **5**, 65–110.
- Richter F. M., Davis A. M., DePaolo D. J. and Watson E. B. (2003) Isotope fractionation by chemical diffusion between molten basalt and rhyolite. *Geochim. Cosmochim. Acta* **67**, 3905–3923.
- Richter F. M., Watson E. B., Mendybaev R., Dauphas N., Georg B., Watkins J. and Valley J. (2009) Isotopic fractionation of the major elements of molten basalt by chemical and thermal diffusion. *Geochim. Cosmochim. Acta* **73**, 4250–4263.
- Rustad J. R., Casey W. H., Yin Q.-Z., Bylaska E. J., Felmy A. R., Bogatko S. A., Jackson V. E. and Dixon D. A. (2010) Isotopic fractionation of $\text{Mg}^{2+}\text{(aq)}$, $\text{Ca}^{2+}\text{(aq)}$, and $\text{Fe}^{2+}\text{(aq)}$ with carbonate minerals. *Geochim. Cosmochim. Acta* **74**, 6301–6323.
- Schauble E. A. (2011) First-principles estimates of equilibrium magnesium isotope fractionation in silicate, oxide, carbonate and hexaaquamagnesium(2+) crystals. *Geochim. Cosmochim. Acta* **75**, 844–869.
- Schauble E. A., Rossman G. R. and Taylor, Jr., H. P. (2004) Theoretical estimates of equilibrium chromium-isotope fractionations. *Chem. Geol.* **205**, 99–114.
- Schauble E. A., Ghosh P. and Eiler J. M. (2006) Preferential formation of C-13-O-18 bonds in carbonate minerals, estimated using first-principles lattice dynamics. *Geochim. Cosmochim. Acta* **70**, 2510–2529.
- Schmitt A. D., Chabaux F. and Stille P. (2003) The calcium riverine and hydrothermal isotopic fluxes and the oceanic calcium mass balance. *Earth Planet. Sci. Lett.* **213**, 503–518.

- Schmitt A.-D., Vigier N., Lemarchand D., Millot R., Stille P. and Chabaux F. (2012) Processes controlling the stable isotope compositions of Li, B, Mg and Ca in plants, soils and waters: a review. *C.R. Geosci.* **344**, 704–722.
- Schmitt A.-D., Cobert F., Bourgeade P., Ertlen D., Labolle F., Gangloff S., Badot P.-M., Chabaux F. and Stille P. (2013) Calcium isotope fractionation during plant growth under a limited nutrient supply. *Geochim. Cosmochim. Acta* **110**, 70–83.
- Seo J.-H., Lee S.-K. and Lee I. (2007) Quantum chemical calculations of equilibrium copper (I) isotope fractionations in ore-forming fluid. *Chem. Geol.* **243**, 225–237.
- Shannon R. D. (1976) Revised effective ionic-radii and systematic studies of interatomic distances in halides and chalcogenides. *Acta Crystallogr. A* **32**, 751–767.
- Sholl D. and Steckel J. A. (2009) *Density Functional Theory: A Practical Introduction*. Wiley.
- Sime N. G., De La Rocha C. L., Tipper E. T., Tripathi A., Galy A. and Bickle M. J. (2007) Interpreting the Ca isotope record of marine biogenic carbonates. *Geochim. Cosmochim. Acta* **71**, 3979–3989.
- Simon J. I. and DePaolo D. J. (2010) Stable calcium isotopic composition of meteorites and rocky planets. *Earth Planet. Sci. Lett.* **289**, 457–466.
- Simon J. I., DePaolo D. J. and Moynier F. (2009) Calcium isotope composition of meteorites, Earth, and Mars. *Astrophys. J.* **702**, 707–715.
- Smyth J. R. . and Bish D. L. (1988) *Crystal Structure and Cation Sites of the Rock Forming Minerals*. Allen & Unwin, Boston.
- Soudry D., Segal I., Nathan Y., Glenn C. R., Halicz L., Lewy Z. and Vonderhaar D. L. (2004) 44Ca/42Ca and 143Nd/144Nd isotope variations in Cretaceous–Eocene Tethyan francolites and their bearing on phosphogenesis in the southern Tethys. *Geology* **32**, 389–392.
- Steuber T. and Buhl D. (2006) Calcium-isotope fractionation in selected modern and ancient marine carbonates. *Geochim. Cosmochim. Acta* **70**, 5507–5521.
- Tossell J. A. (2005) Calculating the partitioning of the isotopes of Mo between oxidic and sulfidic species in aqueous solution. *Geochim. Cosmochim. Acta* **69**, 2981–2993.
- Troullier N. and Martins J. L. (1991) Efficient pseudopotentials for plane-wave calculations. II. Operators for fast iterative diagonalization. *Phys. Rev. B* **43**, 8861–8869.
- Urey H. C. (1947) The thermodynamic properties of isotopic substances. *J. Chem. Soc.*, 562–581.
- Valdes M. C., Moreira M., Foriel J. and Moynier F. (2014) The nature of Earth's building blocks as revealed by calcium isotopes. *Earth Planet. Sci. Lett.* **394**, 135–145.
- Vanderbilt D. (1990) Soft self-consistent pseudopotentials in a generalized eigenvalue formalism. *Phys. Rev. B* **41**, 7892–7895.
- van der Laan S., Zhang Y., Kennedy A. K. and Wyllie P. J. (1994) Comparison of element and isotope diffusion of K and Ca in multicomponent silicate melts. *Earth Planet. Sci. Lett.* **123**, 155–166.
- Wentzcovitch R. M. (1991) Invariant molecular-dynamics approach to structural phase transitions. *Phys. Rev. B* **44**, 2358–2361.
- Wentzcovitch R. M., Yu Y. G. and Wu Z. (2010) Thermodynamic properties and phase relations in mantle minerals investigated by first principles quasiharmonic theory. *Rev. Mineral. Geochim.* **71**, 59–98.
- Wunder B., Meixner A., Romer R. L. and Jahn S. (2011) Li-isotope fractionation between silicates and fluids: pressure dependence and influence of the bonding environment. *Eur. J. Mineral.* **23**, 333–342.
- Yang H. X. and Ghose S. (1995) High-temperature single-crystal X-ray-diffraction Studies of the ortho-proto phase-transition in enstatite, $Mg_2Si_2O_6$ at 1360 K. *Phys. Chem. Miner.* **22**(5), 300–310.
- Young E. D., Tonui E., Manning C. E., Schauble E. and Macris C. A. (2009) Spinel-olivine magnesium isotope thermometry in the mantle and implications for the Mg isotopic composition of Earth. *Earth Planet. Sci. Lett.* **288**, 524–533.
- Zhu P. and Macdougall J. D. (1998) Calcium isotopes in the marine environment and the oceanic calcium cycle. *Geochim. Cosmochim. Acta* **62**, 1691–1698.

Associate editor: Weidong Sun